Supplement

S1. Data processing of CHARON-PTR-ToF-MS

The raw data files of CHARON-PTR-ToF-MS were processed by the Ionicon Data Analyzer (IDA 1.0.2, Ionicon Analytik). Mass calibrations were performed using four ion peaks including H_3O^+ (*m/z*21.022), C_3H_6OH+ (*m/z*59.049), C_6H_5I+ (*m/z*203.943) and $C_6H_5I_2$+ (*m/z* 330.848), where $C_6H_5I^+$ and $C_6H_5I_2^+$ were produced from the internal standard diiodobenzene (Ionicon Analytik). High-resolution peak fitting for each ion was performed automatically by the IDA software and refined manually according to the PTR-ToF-MS literature (Pagonis et al., 2019; Yáñez-Serrano et al., 2021). The quantification procedure of CHARON-PTR-ToF-MS data has been described in detail by (Müller et al., 2017; Leglise et al., 2019). The collision rate (k) between the analyte molecules and PTR reagent ions (H_3O^+) is calculated based on the parametrization method (Su and Chesnavich, 1982; Gioumousis and Stevenson, 1958; Bosque and Sales, 2002). This method uses the properties of the analyte molecule as input parameters: (i) its molecular weight, (ii) its molecular polarizability which is calculated from the elemental composition using the parametrization method and (iii) its dipole moment which is assumed to be 0.3 and 2.75 D for pure and substituted hydrocarbons, respectively. Assuming no interference of fragmentation, the maximum uncertainty of this quantification method is ±40%. The separation of gas and particle measurement data as well as particle background subtractions were performed with the custom-in MATLAB script in IDA. Since the PTR-MS shows slow responses to some organic species especially oxidized species in the particle phase (Piel et al., 2021), the initial 290 s particle-phase data at each CHARON measurement mode were excluded. We also excluded the last 10 s particle-phase data at each CHARON measurement mode to avoid any interference from the switching between different measurement modes. Then the rest of 5 min (300 s) particle data were corrected by the interpolate subtraction of HEPA filter background. An average enrichment factor of ~6 was used for calculating the mass concentrations of particles measured by the CHARON based on the CHARON calibration with ammonium nitrate particles (**Fig. S3**) and the ambient measurements of particle size distribution by the NanoScan SMPS (**Fig. S7**). For the gas phase data, we also excluded the initial 290 s and the last 10 s data at each VOC measurement mode, which could minimize the effect of fluctuated drift tube temperature on instrumental sensitivities during first measurement stage (**Fig. S2a**). Then the rest of 5 min (300 s) gas data were corrected by the

background subtraction from the measurement of VOC-free synthetic air. Finally, we averaged the background-corrected data in gas and particle phases into 5 min presented in this study.

It is well-known that the PTR-MS suffers the ionic fragmentation during the protonation processes (Yuan et al., 2017). According to gas calibrations, the residual fractions were characterized on average ~35% ± 2% and ~37% ± 2% for protonated isoprene ($C_5H_9^+$, *m/z*69.07) and monoterpenes ($C_{10}H_{17}^+$, *m/z*137.13) respectively after their fragmentation within the CHARON-PTR-ToF-MS. A previous study has found that the fragmentation of 2-methyl-3-buten-2-ol (MBO, $C_5H_{11}O^+$) emitted from biogenic sources inside PTR instruments had interferences on the quantification of isoprene based on the $C_5H_9^+$ signals (Karl et al., 2012). As shown in **Fig. S15**, the concentrations of $C_5H_9^+$ were much higher those of $C_5H_{11}O^+$ in both CHARON-PTR-ToF-MS and Vocus-PTR-ToF-MS, and both ions correlated fairly and poorly with each other (r= 0.54 and 0.09). It indicates that the fragmentation of MBO have no significant influence on the attribution of $C_5H_9^+$ to isoprene in this study. Recent studies have found that PTR-measured $C_5H_9^+$ signals can be significantly contributed by the fragmentation of cycloalkanes and long-chain aldehydes (e.g., octanal and nonanal) emitted from anthropogenic sources such as fossil fuel use and cooking in urban regions (Coggon et al., 2023; Pfannerstill et al., 2023). In this study, the concentrations of cycloalkanes and long-chain aldehydes such as octanal ($C_8H_{17}O^+$) and nonanal ($C_9H_{19}O^+$) were two orders of magnitude lower than that of $C_5H_9^+$, thus their interferences were also negligible in this study. Finally, we scaled the measured data of $C_5H_9^+$ and $C_{10}H_{17}^+$ by a factor of 2.86 and 2.70 respectively to quantify the concentrations of isoprene and monoterpenes in this study. For other calibrated species including benzene, toluene, xylenes, trimethylbenzene, methanol and acetone, they have minor fragmentation in CHARON-PTR-ToF-MS. Besides, no fragmentation correction was made for uncalibrated VOC species.

S2. Comparisons of VOCs between CHARON-PTR-ToF-MS and Vocus-PTR-ToF-MS

We first compared the calibrated VOC species measured by the PTR-MS instruments during the entire measurement campaign. As shown in **Fig. S12**, good agreements were observed for $C_6H_7^+$ (benzene), $C_7H_9^+$ (toluene), $C_8H_{11}^+$ (C_8-aromatics) and $C_9H_{13}^+$ (C_9-aromatics) between CHARON-PTR-MS and Vocus-PTR-MS within the differences of 10-30%. It should be noted that $C_5H_9^+$ (isoprene) and $C_{10}H_{17}^+$ (monoterpenes) were fragmented differently inside CHARON-PTR-ToF-

MS and Vocus-PTR-ToF-MS. To take account into fragmentation corrections, we scaled the signals of $C_5H_9^+$ and $C_{10}H_{17}^+$ measured by the CHARON-PTR-ToF-MS with a factor of 2.86 and 2.70 to obtain the concentrations of isoprene and monoterpenes respectively. Similarly, we scaled the signals of $C_5H_9^+$ and $C_{10}H_{17}^+$ measured by the Vocus-PTR-ToF-MS with a factor of 1.25 and 1.67 to obtain the concentrations of isoprene and monoterpenes respectively. Then good agreements were observed for isoprene and monoterpenes between CHARON-PTR-ToF-MS and Vocus-PTR-ToF-MS (**Fig. S12**). We found that $C_3H_7O^+$ (acetone + propanal) measured by CHARON-PTR-ToF-MS were higher than that measured by Vocus- PTR-ToF-MS by a factor of ~2.5. The differences of $C_3H_7O^+$ could be due to PTR-MS fragmentation of higher-molecular-weight VOCs that produce signals at the ion mass of $C_3H_7O^+$ or differences in the detection of acetone and propanal from the two PTR-MS instruments. Besides, the Vocus-PTR-ToF-MS cannot quantify the concentration of methanol (CH_5O^+) due to reduced ion transmission at lower masses (m/z<40), thus no comparison was made.

We also summarized the comparisons of a suite of VOC ions measured by Vocus- PTR-ToF-MS and CHARON- PTR-ToF-MS during the second measurement stage (22^{nd}-30^{th} June) in **Table S4**. More than 75 VOC ions measured by these two PTR-MS instruments showed good correlations ($r > 0.5$). However, the concentrations of these well-correlated VOC ions measured by Vocus-PTR-ToF-MS were generally higher than those measured by CHARON- PTR-ToF-MS by factors of 1-10. Note that the total concentrations of major VOC ions measured by the CHARON-PTR-ToF-MS and the Vocus-PTR-ToF-MS were comparable (**Fig. S5**). Therefore, the differences for individual VOC species could result from the different sensitivities of each VOC species or fragmentation patterns between these two instruments. In addition, we employed different calculation method for the CHARON-PTR-ToF-MS data and the Vocus-PTR-ToF-MS data, which introduced external differences for the comparison of uncalibrated VOC ions.

During the first measurement stage, many VOCs detected by CHARON-PTR-ToF-MS also correlated with those measured by Vocus-PTR-ToF-MS. However, the actual PTR-MS drift tube temperatures were different between the first and second measurement stage, which leads to the disagreement of VOC concentrations over the entire campaign. Here we adopted a simple method to scale the concentrations of selected VOC ions during the first measurement stage. Specifically, the selected VOC ions measured by CHARON- PTR-ToF-MS have good correlations with those measured by Vocus-PTR-ToF-MS during both measurement stages. Then we scaled the

concentrations of each selected VOC ions based on the slope differences of first measurement stage to second one. This simple correction method was validated with the calibrated VOC species (**Fig. S12**) and useful for other uncalibrated VOC species like oxygenated VOCs and green leaf volatiles (GLV) species (**Figs. S13 and S14**). Therefore, we can present a consistent VOC data set measured by CHARON-PTR-ToF-MS for the entire campaign.

Table S1. Overview of instruments deployed in the measurement container.

Measured parameters	Instruments	Measurement period
Meteorological parameters	WS700 (Lufft GmbH)	06/05-06/30, 2020
O_3	Cranox II (Eco Physics®)	06/10-06/30, 2020
CO, CO_2, CH_4, H_2O	CRDS (G2401, Picarro Inc.)	06/10-06/30, 2020
Particle number concentration (> 2.5 nm)	CPC3776 (TSI Inc.)	06/05-06/12, 2020
Particle size distribution (10-410 nm)	NanoScan SMPS3910 (TSI Inc.)	06/05-06/30, 2020
Black carbon (BC)	MA200 (AethLabs Inc.)	06/05-06/30, 2020
Particle concentration ($PM_{2.5}$ and PM_{10})	Fidas200 (Palas GmbH)	06/05-06/30, 2020
VOCs and semi-volatile particles	CHARON-PTR-ToF-MS (IONICON GmbH)	06/05-06/30, 2020
VOCs and oxygenated VOCs	Vocus-PTR-ToF-MS (Aerodyne Research Inc.)	06/10-06/30, 2020

Table S2. Compositions of gas standard for the calibrations of CHARON-PTR-ToF-MS and Vocus-PTR-ToF-MS.

IONICON certificated gas standard		FZJ home-made gas standard	
Components	Conc. (ppb)	Components	Conc. (ppb)
methanol	98.5 ± 9.1	methanol	867.7 ± 61.7
acetone	98.0 ± 9.1	acetonitrile	865.4 ± 61.5
isoprene	103.0 ± 9.5	acetaldehyde	1229.3 ± 87.4
benzene	94.0 ± 8.7	isoprene	815.5 ± 58.0
toluene	97.0 ± 9.0	benzene	946.7 ± 67.3
o-xylene	102.0 ± 9.4	toluene	945.4 ± 67.2
p-xylene	98.3 ± 9.1	o-xylene	946.3 ± 67.3
m-xylene	94.1 ± 8.8	chlorobenzene	962.8 ± 68.4
1,3,5-trimethylbenzene	108.0 ± 9.9	α-pinene	845.5 ± 60.1
α-pinene	101.0 ± 9.3	1-butanol	859.8 ± 61.1
limonene	95.0 ± 8.8	acetone	1181.5 ± 84.0
		2-butanone	1026.4 ± 73.0
		3-pentanone	1045.1 ± 74.3
		methyl vinyl ketone	1018.4 ± 72.4
		(1R)-(+)-norpinone	502.9 ± 35.8

99

Table S3. List of 157 VOC ions measured by the Vocus-PTR-ToF-MS included for the PMF analysis

VOC Ion mass (m/z)	Ion formula	Suggested compounds	Averaged mixing ratio (ppb)	Standard deviation
41.039	$C_3H_5^+$	fragment	0.1852	0.4618
42.034	$C_2H_4N^+$	acetonitrile	0.0402	0.0213
43.018	$C_2H_3O^+$	fragment	0.3649	0.2289
43.054	$C_3H_7^+$	fragment	0.2127	0.5983
47.049	$C_2H_7O^+$	ethanol	0.2840	0.3444
53.002	C_3HO^+	unknown	0.0252	0.0379
53.039	$C_4H_5^+$	fragment	0.0092	0.0076
57.033	$C_3H_5O^+$	acrolein	0.1823	0.2125
58.041	$C_3H_6O^+$	acetone charged transfer	0.0030	0.0019
59.049	$C_3H_7O^+$	acetone	2.0768	0.7845
61.028	$C_2H_5O_2^+$	acetic acid	1.1125	0.6110
63.023	$C_5H_3^+$	unknown	0.0113	0.0150
65.023	$CH_5O_3^+$	unknown	0.0011	0.0009
66.046	$C_5H_6^+$	C_5H_7 charged transfer	0.0015	0.0019
67.054	$C_5H_7^+$	fragment	0.0282	0.0234
68.062	$C_5H_8^+$	C_5H_9 charged transfer	0.0019	0.0024
69.033	$C_4H_5O^+$	furan	0.0097	0.0062
69.07	$C_5H_9^+$	isoprene	0.4223	0.3694
70.041	$C_4H_6O^+$	C_4H_7O charged transfer	0.0006	0.0004
71.049	$C_4H_7O^+$	MVK/methacrolein	0.1870	0.1122
73.028	$C_3H_5O_2^+$	methyl glyoxal/acrylic acid	0.0467	0.0430
73.065	$C_4H_9O^+$	MEK/butanal	0.2158	0.1518
75.044	$C_3H_7O_2^+$	acetone water cluster	0.2679	0.1299
77.023	$C_2H_5O_3^+$	glycolic acid	0.0172	0.0167
77.06	$C_3H_9O_2^+$	ethylene glycol	0.5114	0.1969
79.039	$C_2H_7O_3^+$	acetic acid cluster	0.4875	0.3103
79.054	$C_6H_7^+$	benzene	0.0889	0.0788
81.07	$C_6H_9^+$	monoterpene fragment	0.4589	0.6799
83.049	$C_5H_7O^+$	methyl furan	0.0323	0.0176
83.086	$C_6H_{11}^+$	fragment	0.0503	0.0488
85.028	$C_4H_5O_2^+$	furanone/hydroxy furan	0.0217	0.0141
85.065	$C_5H_9O^+$	methylcyclopentane	0.0322	0.0161
86.073	$C_5H_{10}O^+$	$C_5H_{11}O$ charged transfer	0.0004	0.0002
87.044	$C_4H_7O_2^+$	2,3-butanedione/butyrolacetone	0.1783	0.1107
87.08	$C_5H_{11}O^+$	pentanal/pentanone/3-methylbutanal/allyl ehtyl ether	0.0399	0.0490
89.06	$C_4H_9O_2^+$	ethyl acetate/butanoic acid	0.2904	0.2370
91.039	$C_3H_7O_3^+$	lactic acid	0.0260	0.0144
91.054	$C_7H_7^+$	fragment	0.0171	0.0152
91.075	$C_4H_{11}O_2^+$	water cluster of C_4H_9O	0.0645	0.0732
92.062	$C_7H_8^+$	toluene charged transfer	0.0060	0.0068

93.018	$C_2H_5O_4^+$	unknown	0.0008	0.0007
93.055	$C_3H_9O_3^+$	propionic acid water cluster	0.0363	0.0170
93.07	$C_7H_9^+$	toluene	0.1096	0.0742
95.034	$C_2H_7O_4^+$	unknown	0.0074	0.0058
95.049	$C_6H_7O^+$	phenol	0.0747	0.0581
95.086	$C_7H_{11}^+$	monoterpene fragment	0.0364	0.0420
97.028	$C_5H_5O_2^+$	furfural	0.0276	0.0195
97.065	$C_6H_9O^+$	2-ethylfuran/2,5-dimethylfuran	0.0166	0.0073
97.101	$C_7H_{13}^+$	fragment	0.0116	0.0142
99.044	$C_5H_7O_2^+$	furfuryl alcohol	0.0537	0.0329
99.08	$C_6H_{11}O^+$	cyclohexannone	0.0293	0.0173
101.06	$C_5H_9O_2^+$	methyl methacrylate	0.0971	0.0551
101.096	$C_6H_{13}O^+$	hexanals/hexanones	0.0177	0.0105
103.039	$C_4H_7O_3^+$	acetic anhydride	0.0328	0.0169
103.075	$C_5H_{11}O_2^+$	butanonate	0.0177	0.0092
105.033	$C_7H_5O^+$	C_7 1-oxy 6 DBE	0.0030	0.0023
105.055	$C_4H_9O_3^+$	multiple	0.0295	0.0166
105.091	$C_5H_{13}O_2^+$	1,5-pentanediol	0.0190	0.0140
106.078	$C_8H_{10}^+$	C_8 aromatic charged transfer	0.0010	0.0008
107.086	$C_8H_{11}^+$	C_8 aromatics	0.0523	0.0411
109.065	$C_7H_9O^+$	cresol	0.0101	0.0075
109.101	$C_8H_{13}^+$	terpene fragment	0.0139	0.0249
111.044	$C_6H_7O_2^+$	catechol/benzene diol	0.0406	0.0319
111.08	$C_7H_{11}O^+$	multiple	0.0149	0.0111
113.023	$C_5H_5O_3^+$	unknown	0.0188	0.0131
113.06	$C_6H_9O_2^+$	unknown	0.0214	0.0108
113.096	$C_7H_{13}O^+$	ethyl cyclopentanone/	0.0081	0.0049
115.039	$C_5H_7O_3^+$	C_5 3-oxy 3D BE	0.0127	0.0090
115.075	$C_6H_{11}O_2^+$	C_6 diketone isomers/vinylethyl acetate	0.0338	0.0188
115.112	$C_7H_{15}O^+$	dimethylpentanone/heptanone	0.0066	0.0050
117.055	$C_5H_9O_3^+$	C_5 3-oxy 2D BE isomers	0.0350	0.0148
117.091	$C_6H_{13}O_2^+$	ethyl butyrate	0.0171	0.0158
119.034	$C_4H_7O_4^+$	succinic acid	0.1406	0.1318
121.101	$C_9H_{13}^+$	C_9 aromatics	0.0343	0.0286
123.044	$C_7H_7O_2^+$	benzoic acid	0.0151	0.0101
123.08	$C_8H_{11}O^+$	methylanisole	0.0030	0.0015
123.117	$C_9H_{15}^+$	terpene fragment	0.0086	0.0052
125.096	$C_8H_{13}O^+$	C_4 substituted furan	0.0080	0.0043
129.091	$C_7H_{13}O_2^+$	allyl ester isobutyric acid	0.0166	0.0091
129.127	$C_8H_{17}O^+$	octanal	0.0146	0.0120
131.034	$C_5H_7O_4^+$	isoprene oxidation product	0.0127	0.0074
131.07	$C_6H_{11}O_3^+$	multiple	0.0169	0.0124
131.107	$C_7H_{15}O_2^+$	C_7 carboxylic acid	0.0045	0.0023

133.05	$C_5H_9O_4^+$	glutaric acid	0.0160	0.0096
133.101	$C_{10}H_{13}^+$	multiple	0.0056	0.0045
136.125	$C_{10}H_{16}^+$	monoterpene charged transfer	0.0039	0.0057
137.132	$C_{10}H_{17}^+$	monoterpenes	0.8682	1.4585
139.075	$C_8H_{11}O_2^+$	2-methoxy-4-methylphenol	0.0040	0.0028
139.112	$C_9H_{15}O^+$	monoterpene oxidation product (e.g., nopinone)	0.0527	0.0368
141.055	$C_7H_9O_3^+$	methoxycatechol	0.0066	0.0033
141.091	$C_8H_{13}O_2^+$	unknown	0.0075	0.0044
141.127	$C_9H_{17}O^+$	trans-2-nonenal	0.0056	0.0029
143.07	$C_7H_{11}O_3^+$	unknown	0.0062	0.0036
143.107	$C_8H_{15}O_2^+$	unknown	0.0128	0.0101
143.143	$C_9H_{19}O^+$	nonanal/2-nonanone	0.0341	0.0299
145.086	$C_7H_{13}O_3^+$	unknown	0.0058	0.0029
145.122	$C_8H_{17}O_2^+$	ethyl hexanoate	0.0033	0.0018
147.065	$C_6H_{11}O_4^+$	unknown	0.0072	0.0042
149.023	$C_8H_5O_3^+$	phthalic anhydride	0.0019	0.0018
149.096	$C_{10}H_{13}O^+$	unknown	0.0034	0.0030
149.132	$C_{11}H_{17}^+$	sesquiterpene fragment	0.0013	0.0011
151.075	$C_9H_{11}O_2^+$	vinyl guaiacol/benzyl acetate	0.0015	0.0009
151.112	$C_{10}H_{15}O^+$	monoterpene oxidation product (e.g., pinonaldehyde fragment)	0.0244	0.0165
153.055	$C_8H_9O_3^+$	methyl salicylate	0.0179	0.0081
153.091	$C_9H_{13}O_2^+$	unknown	0.0050	0.0027
153.127	$C_{10}H_{17}O^+$	camphor/monoterpene oxidation product	0.0230	0.0150
155.07	$C_8H_{11}O_3^+$	syringol	0.0025	0.0016
155.107	$C_9H_{15}O_2^+$	monoterpene oxidation product	0.0060	0.0044
155.143	$C_{10}H_{19}O^+$	linalool	0.0091	0.0130
157.086	$C_8H_{13}O_3^+$	monoterpene oxidation product (e.g., terpenylic acid)	0.0057	0.0032
157.122	$C_9H_{17}O_2^+$	C_9 2-oxy 2DBE isomers	0.0110	0.0064
157.159	$C_{10}H_{21}O^+$	menthol-type monoterpenes/ decanal	0.0189	0.0471
159.065	$C_7H_{11}O_4^+$	3,6-oxoheptanoic acid	0.0045	0.0024
159.102	$C_8H_{15}O_3^+$	monoterpene oxidation product	0.0046	0.0036
159.138	$C_9H_{19}O_2^+$	methyl octanoate	0.0027	0.0015
161.081	$C_7H_{13}O_4^+$	unknown	0.0032	0.0019
165.055	$C_9H_9O_3^+$	unknown	0.0007	0.0006
167.034	$C_8H_7O_4^+$	terephthalic acid	0.0047	0.0034
167.107	$C_{10}H_{15}O_2^+$	monoterpene oxidation product	0.0063	0.0033
169.05	$C_8H_9O_4^+$	C_8 4-oxy 5-DBE	0.0006	0.0005
169.086	$C_9H_{13}O_3^+$	C_9 3-oxy 4-DBE	0.0021	0.0013
169.122	$C_{10}H_{17}O_2^+$	monoterpene oxidation product (e.g pinonaldehyde)	0.0216	0.0160
171.029	$C_7H_7O_5^+$	unknown	0.0014	0.0011
171.065	$C_8H_{11}O_4^+$	unknown	0.0012	0.0006

171.102	$C_9H_{15}O_3^+$	monoterpene oxidation product	0.0048	0.0024
171.138	$C_{10}H_{19}O_2^+$	linalool oxide	0.0066	0.0040
173.044	$C_7H_9O_5^+$	toluene oxidation product	0.0007	0.0005
173.081	$C_8H_{13}O_4^+$	monoterpene oxidation product	0.0020	0.0013
173.117	$C_9H_{17}O_3^+$	unknown	0.0014	0.0016
173.154	$C_{10}H_{21}O_2^+$	unknown	0.0016	0.0011
175.06	$C_7H_{11}O_5^+$	unknown	0.0024	0.0013
175.096	$C_8H_{15}O_4^+$	monoterpene oxidation product	0.0014	0.0009
183.102	$C_{10}H_{15}O_3^+$	monoterpene oxidation product	0.0026	0.0014
185.117	$C_{10}H_{17}O_3^+$	monoterpene oxidation product (e.g., *cis*-pinonic acid)	0.0066	0.0037
185.154	$C_{11}H_{21}O_2^+$	unknown	0.0007	0.0004
187.096	$C_9H_{15}O_4^+$	monoterpene oxidation product (e.g., pinic acid)	0.0018	0.0009
189.076	$C_8H_{13}O_5^+$	monoterpene oxidation product	0.0009	0.0005
189.149	$C_{10}H_{21}O_3^+$	unknown	0.0002	0.0002
193.159	$C_{13}H_{21}O^+$	unknown	0.0004	0.0010
195.138	$C_{12}H_{19}O_2^+$	unknown	0.0004	0.0002
197.081	$C_{10}H_{13}O_4^+$	unknown	0.0003	0.0002
197.117	$C_{11}H_{17}O_3^+$	unknown	0.0004	0.0002
197.154	$C_{12}H_{21}O_2^+$	unknown	0.0002	0.0002
199.096	$C_{10}H1_5O_4^+$	monoterpene oxidation product	0.0010	0.0005
199.133	$C_{11}H_{19}O_3^+$	unknown	0.0007	0.0003
201.112	$C_{10}H_{17}O_4^+$	monoterpene oxidation product	0.0011	0.0006
203.091	$C_9H_{15}O_5^+$	monoterpene oxidation product	0.0004	0.0003
203.128	$C_{10}H_{19}O_4^+$	unknown	0.0002	0.0002
205.071	$C_8H_{13}O_6^+$	monoterpene oxidation product	0.0003	0.0002
205.195	$C_{15}H_{25}^+$	sesquiterpenes	0.0039	0.0037
209.154	$C_{13}H_{21}O_2^+$	unknown	0.0004	0.0003
213.076	$C_{10}H_{13}O_5^+$	monoterpene oxidation product	0.0002	0.0001
215.091	$C_{10}H_{15}O_5^+$	monoterpene oxidation product	0.0003	0.0002
215.128	$C_{11}H_{19}O_4^+$	unknown	0.0002	0.0002
217.107	$C_{10}H_{17}O_5^+$	monoterpene oxidation product	0.0003	0.0001
217.143	$C_{11}H_{21}O_4^+$	unknown	0.0001	0.0001
223.169	$C_{14}H_{23}O_2^+$	sesquiterpene oxidation product	0.0003	0.0011

100

Table S4. Comparison of 112 VOC ions measured by Vocus-PTR-ToF-MS to those measured by CHARON-PTR-ToF-MS during second measurement period (22nd-30th June 2020).

No.	VOC ions	Pearson's r	Slope	Intercept	No.	VOC ions	Pearson's r	Slope	Intercept
1	$C_3H_5^+$	0.10	0.002	0.097	57	$C_7H_{13}O_2^+$	**0.86**	2.170	0.002
2	$C_3H_7^+$	0.08	0.004	0.077	58	$C_8H_{17}O^+$	0.01	0.119	0.012
3	$C_2H_7O^+$	**0.74**	4.405	0.083	59	$C_5H_7O_4^+$	**0.67**	3.582	-0.008
4	$C_4H_5^+$	0.38	0.038	0.011	60	$C_6H_{11}O_3^+$	0.11	2.379	0.013
5	$C_3H_7O^+$	**0.82**	0.429	0.030	61	$C_7H_{15}O_2^+$	**0.65**	2.148	0.004
6	$C_2H_5O_2^+$	**0.81**	0.849	-0.164	62	$C_5H_9O_4^+$	0.18	1.535	0.017
7	$CH_5O_3^+$	-0.31	-0.036	0.001	63	$C_{10}H_{13}^+$	**0.54**	0.307	0.003
8	$C_5H_7^+$	0.41	0.110	0.019	64	$C_{10}H_{17}^+$	**0.59**	0.559	0.252
9	$C_4H_5O^+$	0.39	0.205	0.004	65	$C_8H_{11}O_2^+$	0.41	0.239	0.003
10	$C_5H_9^+$	**0.92**	1.652	0.025	66	$C_9H_{15}O^+$	**0.93**	2.903	0.001
11	$C_4H_7O^+$	**0.94**	1.292	-0.002	67	$C_7H_9O_3^+$	**0.69**	0.543	0.001
12	$C_3H_5O_2^+$	**0.75**	0.775	-0.021	68	$C_8H_{13}O_2^+$	**0.76**	1.004	0.003
13	$C_4H_9O^+$	**0.96**	2.256	-0.053	69	$C_9H_{17}O^+$	**0.55**	2.281	0.000
14	$C_3H_7O_2^+$	**0.89**	2.842	-0.001	70	$C_7H_{11}O_3^+$	**0.73**	1.841	0.001
15	$C_3H_9O_2^+$	**0.50**	16.469	0.185	71	$C_8H_{15}O_2^+$	0.17	1.030	0.008
16	$C_6H_7^+$	0.33	0.313	0.079	72	$C_9H_{19}O^+$	0.20	22.151	0.021
17	$C_6H_9^+$	**0.55**	0.201	0.188	73	$C_7H_{13}O_3^+$	**0.68**	5.837	0.005
18	$C_5H_7O^+$	**0.82**	0.987	0.002	74	$C_8H_{17}O_2^+$	**0.53**	1.393	0.005
19	$C_6H_{11}^+$	0.21	0.910	0.039	75	$C_6H_{11}O_4^+$	**0.54**	3.029	0.003
20	$C_4H_5O_2^+$	**0.71**	0.629	-0.004	76	$C_8H_5O_3^+$	**0.72**	0.256	0.001
21	$C_5H_9O^+$	**0.82**	1.702	0.004	77	$C_{10}H_{13}O^+$	**0.76**	0.627	-0.001
22	$C_4H_7O_2^+$	**0.72**	4.300	-0.051	78	$C_{11}H_{17}^+$	0.37	0.311	0.002
23	$C_5H_{11}O^+$	0.44	3.108	0.005	79	$C_9H_{11}O_2^+$	0.48	0.254	0.001
24	$C_4H_9O_2^+$	**0.66**	17.104	-0.112	80	$C_{10}H_{15}O^+$	**0.87**	1.911	0.006
25	$C_3H_7O_3^+$	0.23	0.347	0.023	81	$C_8H_9O_3^+$	**0.85**	1.025	0.004
26	$C_4H_{11}O_2^+$	**0.77**	15.001	-0.273	82	$C_9H_{13}O2^+$	-0.04	-0.048	0.006
27	$C_7H_9^+$	**0.66**	0.499	0.056	83	$C_{10}H_{17}O^+$	**0.85**	1.374	0.003
28	$C_6H_7O^+$	**0.50**	3.027	-0.045	84	$C_8H_{11}O_3^+$	**0.88**	0.355	0.000
29	$C_7H_{11}^+$	0.45	0.103	0.023	85	$C_9H_{15}O_2^+$	0.37	1.035	0.006
30	$C_5H_5O_2^+$	**0.53**	0.967	-0.005	86	$C_{10}H_{19}O^+$	0.05	0.506	0.003
31	$C_6H_9O^+$	**0.77**	0.405	0.005	87	$C_8H_{13}O_3^+$	0.46	2.795	0.005

32	$C_7H_{13}^+$	0.07	0.220	0.015	88	$C_9H_{17}O_2^+$	**0.62**	2.958	0.003
33	$C_5H_7O_2^+$	**0.62**	1.275	-0.001	89	$C_{10}H_{21}O^+$	0.11	25.598	0.019
34	$C_6H_{11}O^+$	**0.91**	3.464	0.001	90	$C_7H_{11}O_4^+$	**0.81**	2.565	-0.001
35	$C_5H_9O_2^+$	**0.52**	1.931	0.039	91	$C_9H_9O_3^+$	**0.53**	0.327	0.000
36	$C_6H_{13}O^+$	**0.77**	6.056	-0.003	92	$C_8H_7O_4^+$	**0.64**	3.022	-0.003
37	$C_4H_7O_3^+$	**0.80**	4.988	-0.008	93	$C_{10}H_{15}O_2^+$	**0.79**	1.203	0.001
38	$C_5H_{11}O_2^+$	**0.71**	2.424	0.009	94	$C_8H_9O_4^+$	**0.53**	0.147	0.000
39	$C_8H_{11}^+$	**0.85**	0.861	0.016	95	$C_9H_{13}O_3^+$	**0.67**	0.543	0.001
40	$C_7H_9O_1^+$	**0.50**	0.664	0.006	96	$C_{10}H_{17}O_2^+$	**0.57**	8.491	-0.004
41	$C_8H_{13}^+$	0.10	0.172	0.015	97	$C_7H_7O_5^+$	0.17	0.367	0.002
42	$C_6H_7O_2^+$	**0.64**	2.227	-0.010	98	$C_8H_{11}O_4^+$	**0.69**	0.132	0.000
43	$C_7H_{11}O^+$	**0.85**	1.352	0.000	99	$C_9H_{15}O_3^+$	**0.57**	1.675	0.005
44	$C_5H_5O_3^+$	**0.74**	0.843	0.002	100	$C_7H_9O_5^+$	0.39	0.274	0.000
45	$C_6H_9O_2^+$	**0.88**	1.172	-0.004	101	$C_8H_{13}O_4^+$	**0.74**	0.982	0.000
46	$C_7H_{13}O^+$	**0.89**	3.037	0.003	102	$C_{10}H_{21}O_2^+$	0.23	0.208	0.002
47	$C_5H_7O_3^+$	0.26	0.381	0.004	103	$C_7H_{11}O_5^+$	**0.71**	1.546	0.001
48	$C_6H_{11}O_2^+$	**0.91**	2.246	-0.001	104	$C_8H_{15}O_4^+$	0.37	1.602	0.001
49	$C_7H_{15}O^+$	**0.63**	3.979	0.001	105	$C_{10}H_{15}O_3^+$	**0.72**	0.867	0.000
50	$C_5H_9O_3^+$	**0.70**	8.684	0.004	106	$C_{10}H_{17}O_3^+$	0.23	0.819	0.006
51	$C_6H_{13}O_2^+$	0.42	4.490	0.015	107	$C_9H_{15}O_4^+$	0.48	0.607	0.001
52	$C_9H_{13}^+$	**0.82**	0.826	0.008	108	$C_8H_{13}O_5^+$	**0.77**	0.589	0.000
53	$C_7H_7O_2^+$	**0.61**	0.982	0.003	109	$C_{10}H_{13}O_4^+$	0.37	0.071	0.000
54	$C_8H_{11}O^+$	**0.73**	0.387	0.001	110	$C_{10}H_{15}O_4^+$	**0.53**	0.097	0.000
55	$C_9H_{15}^+$	**0.66**	0.583	0.004	111	$C_{15}H_{25}^+$	**0.71**	0.554	-0.001
56	$C_8H_{13}O^+$	**0.59**	0.910	0.003	112	$C_{10}H_{15}O_5^+$	**0.87**	0.147	0.002

The Pearson's r was >0.5 in bold.

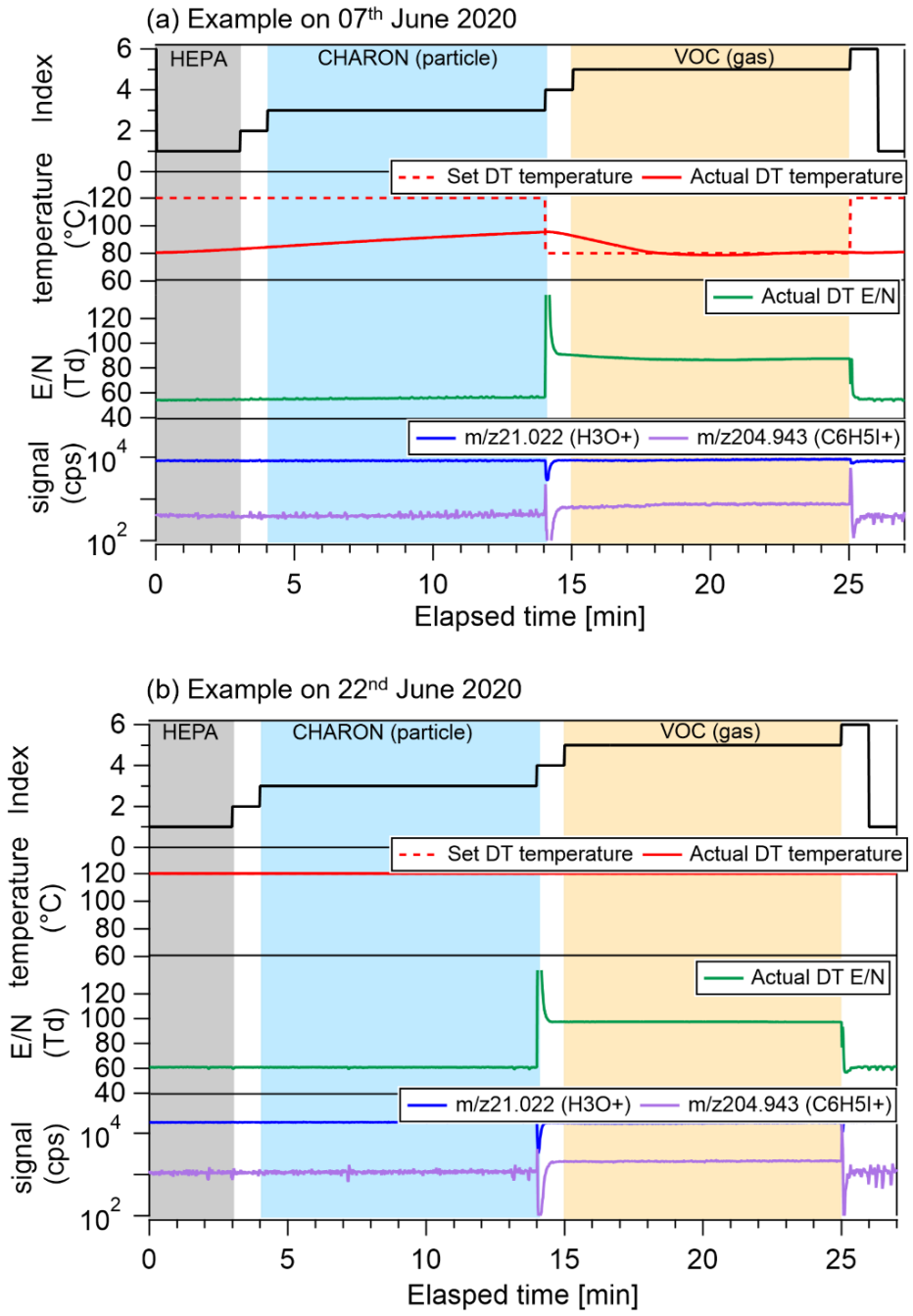

Figure S1. Examples of alternatingly measurement cycle in the CHARON-PTR-ToF-MS on (a) 7th of June and (b) 22nd of June 2020. Time series of PTR mode index, set and actual PTR drift tube (DT) temperature, actual DT E/N value, reagent ion (H_3O^+) and mass calibration ion ($C_6H_5I^+$) for the examples.

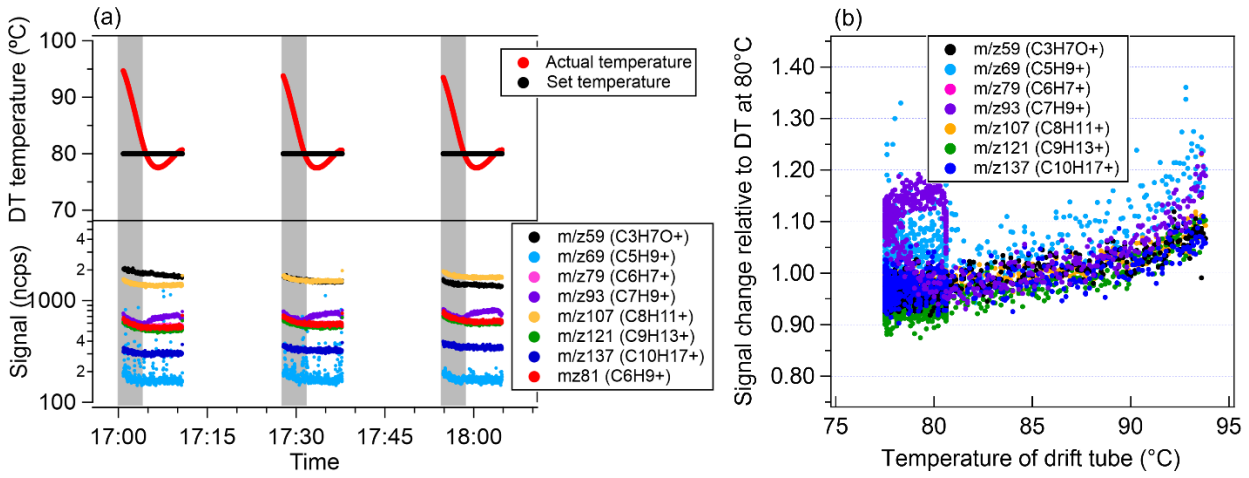

Figure S2. Three alternatingly measurement cycles for the ~100 times diluted IONICON gas cylinder by the CHARON-PTR-ToF-MS with the same setting during first measurement stage (5th-19th of June 2020) of field campaign. (a) Time series of set and actual PTR drift tube (DT) temperature and the normalized calibrated VOC signals. The grey shaded areas mark the first 4 minutes when the actual DT temperature was rapidly changed back to ~80 °C. (b) Signal change of VOCs relative to those measured with DT temperature at 80 °C.

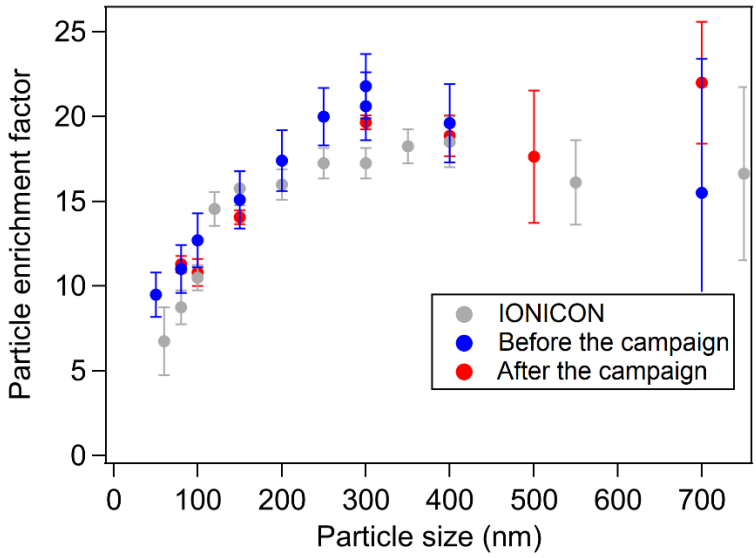

Figure S3. CHARON inlet calibrated enrichment factor of ammonium nitrate as a function of particle size in the 60-700 nm range before and after the measurement campaign in comparison to the enrichment factor certificated by the IONICON.

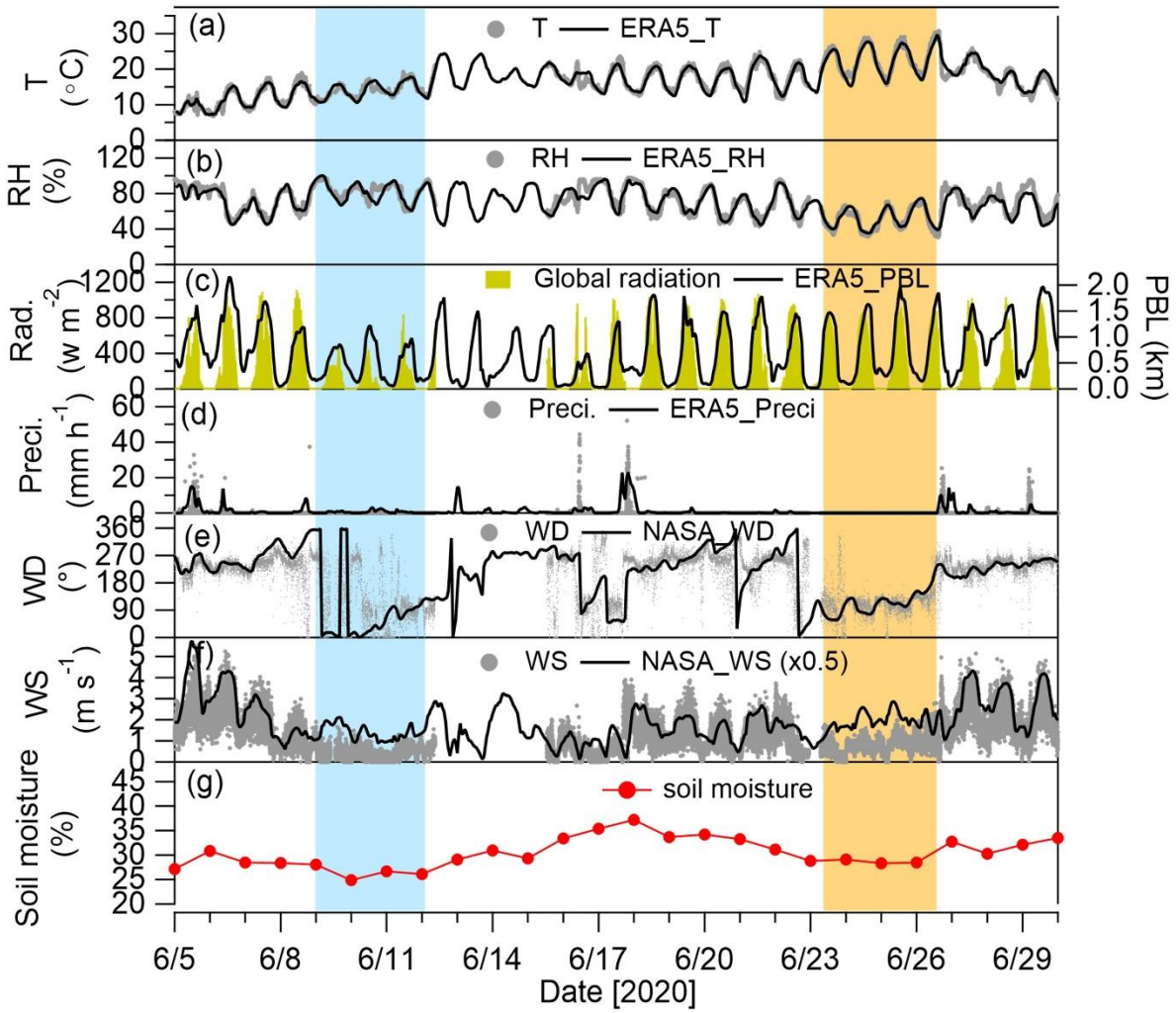

Figure S4. Time series of meteorological data measured by the WS700 sensor and hourly data of temperature (T), relative humidity (RH), precipitation (Preci.) and planetary boundary layer (PBL) height obtained from ERA5 reanalysis and hourly data of wind direction and speed (WD and WS) obtained from NASA Power Data Access Viewer. The blue and yellow shaded areas mark low-T and high-T episodes. (g) The daily soil moisture measured by a cosmic ray neutron sensor which was located ~ 150 m southwest of the sampling site.

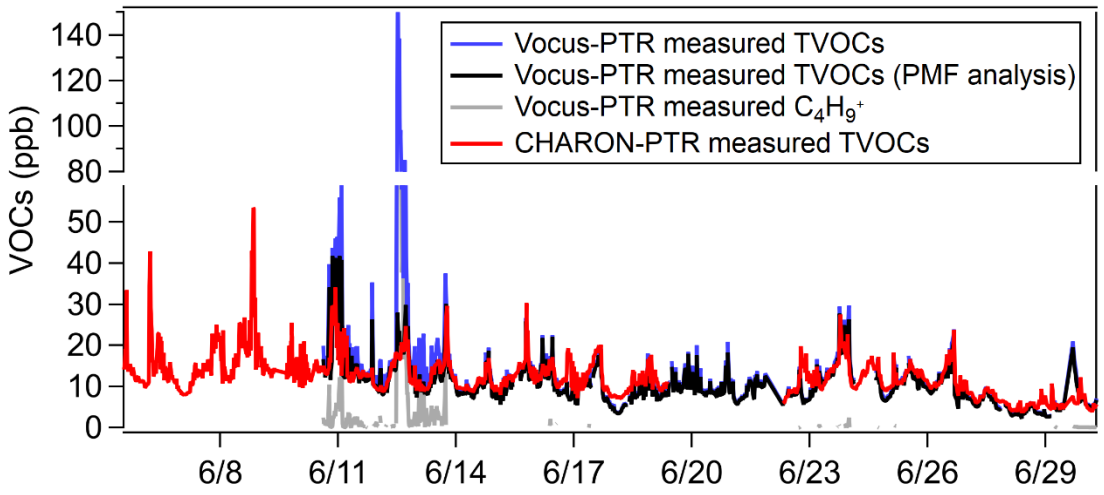

131

132 **Figure S5.** Time series of all VOCs (blue), 157 VOCs ions for the PMF analysis (black) and $C_4H_9^+$
133 that measured by the Vocus-PTR-ToF-MS. The major VOCs measured by the CHARON-PTR-
134 ToF-MS (red) was shown for the comparison.

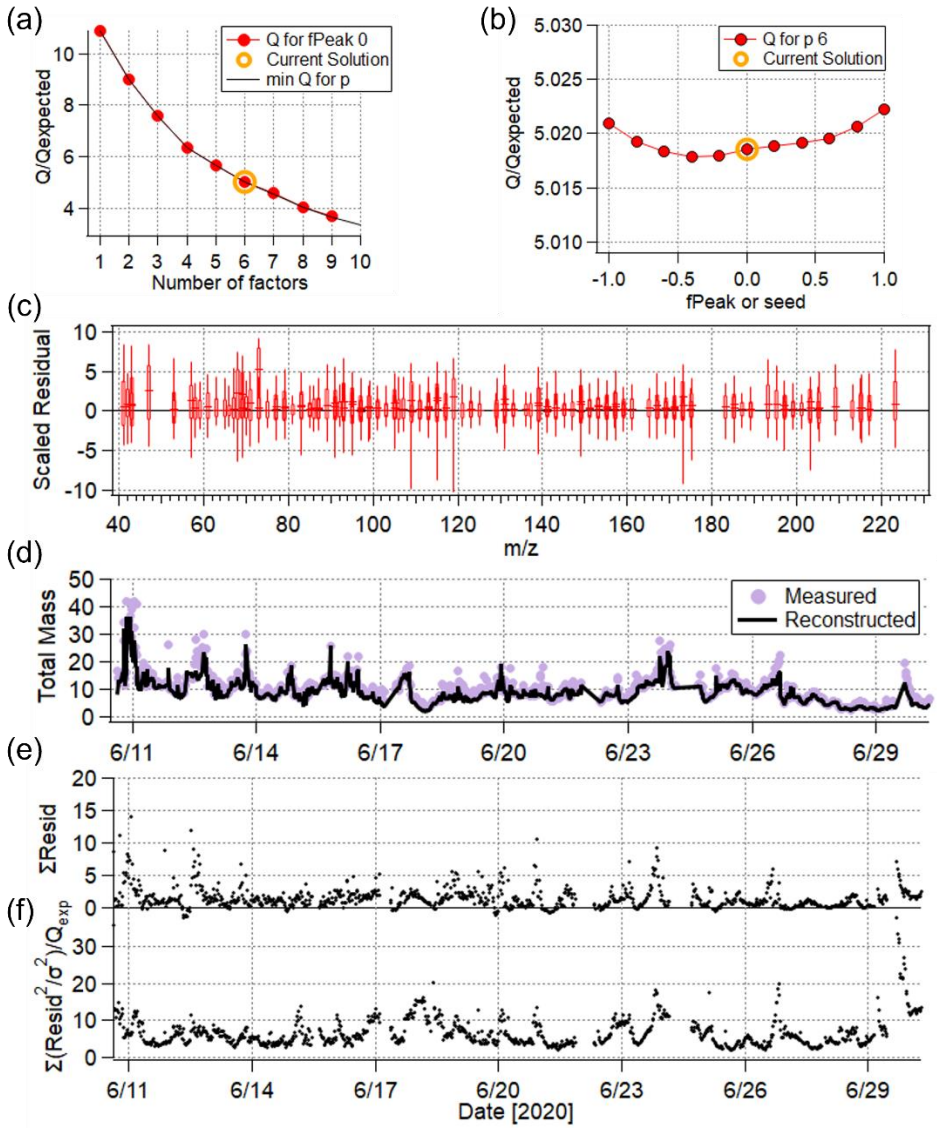

Figure S6. A summary of diagnostic plots for the PMF analysis of Vocus-PTR-ToF-MS mass spectral data: (a) Q/Q_{exp} as a function of number of factors; (b) Q/Q_{exp} as a function of f_{peak} or seed values; (c) scaled residual for each VOC ion; (d) comparison of measured and PMF reconstructed mass; (e-f) time series of residual and Q/Q_{exp} values.

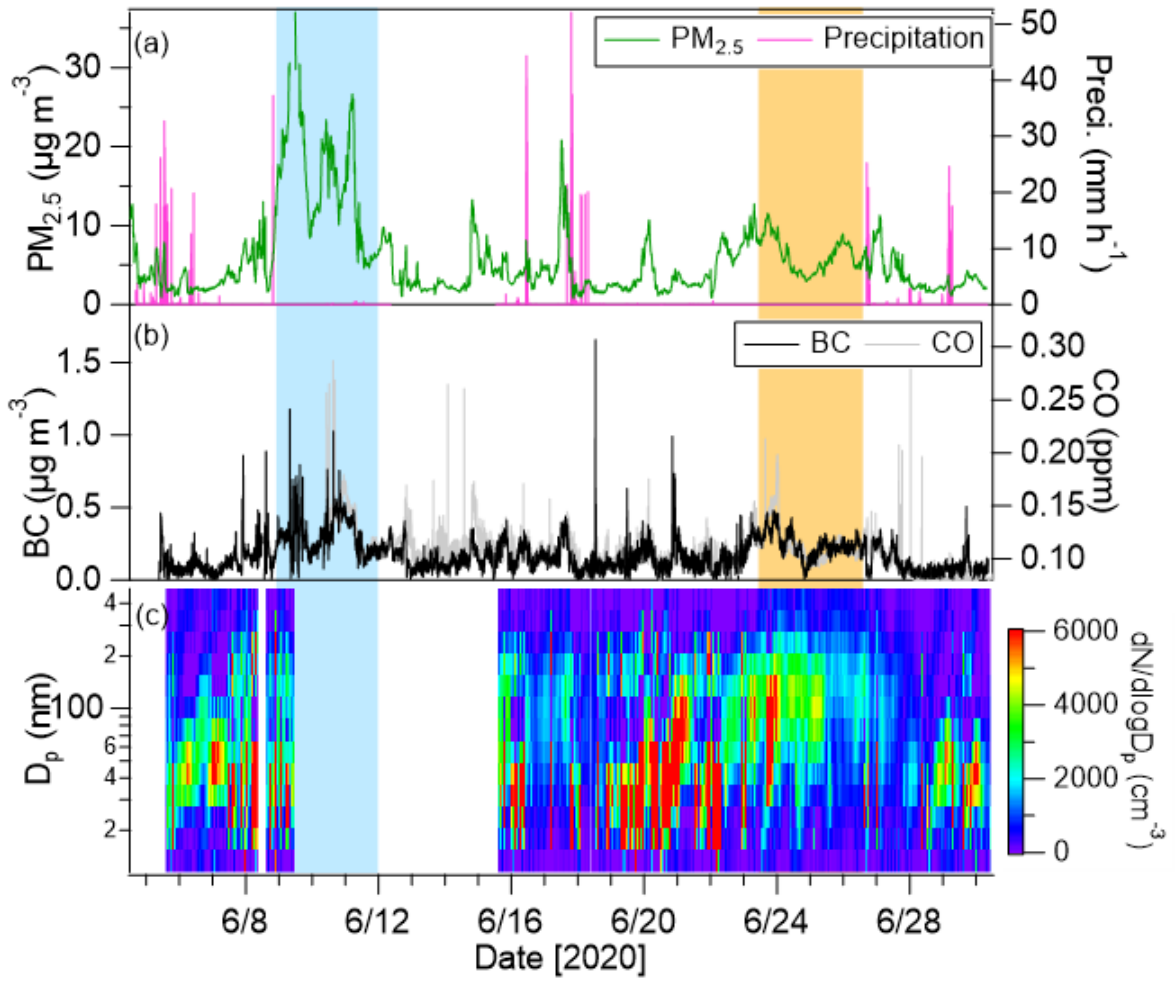

Figure S7. Time series of (a) $PM_{2.5}$ mass concentrations and precipitation, (b) BC mass concentrations and CO. (c) particle number size distributions measured by the NanoScan SMPS. The blue and yellow shaded areas mark low-T and high-T episodes.

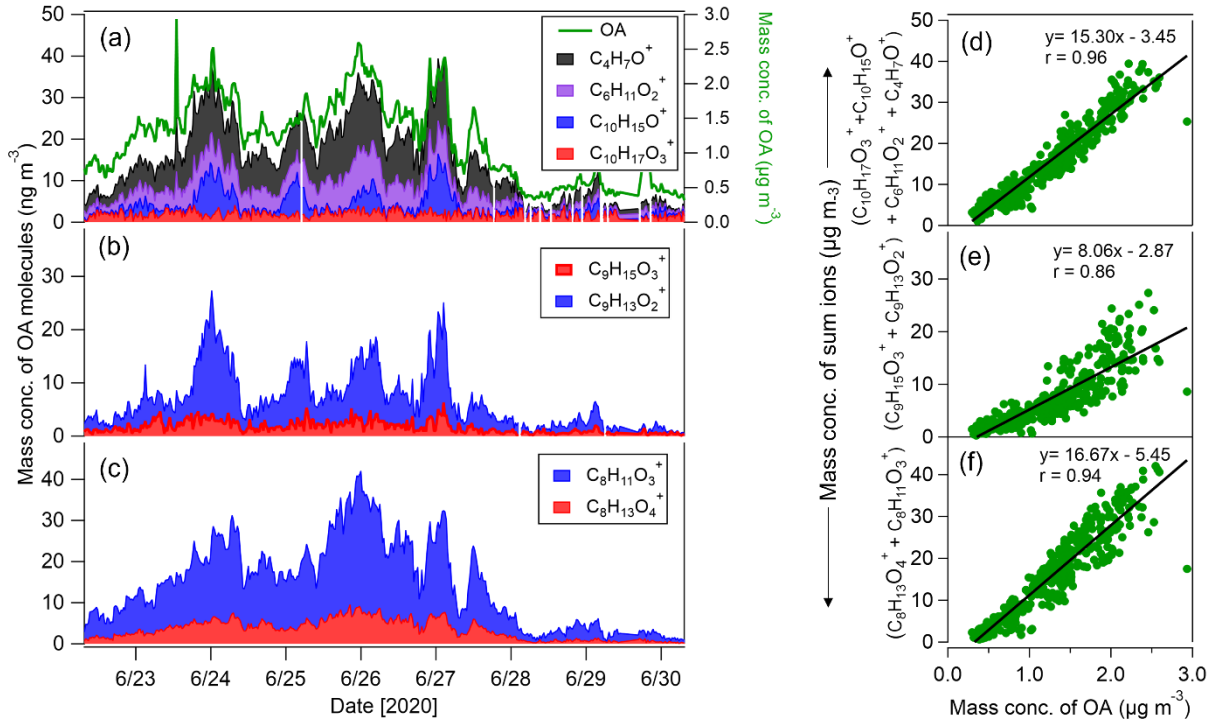

Figure S8. Time series of mass concentrations of organic aerosol (OA) and parent organic molecules and its fragment ions from monoterpene oxidation measured by the CHARON-PTR-ToF-MS: (a) $C_{10}H_{17}O_3^+$ (cis-pinonic acid); (b) $C_9H_{15}O_3^+$ (norpinonic acid and its isomers) (c) $C_8H_{13}O_4^+$ (norpinic acid and its isomers). (d-f) scatter plots of OA vs. *cis*-pinonic acid, norpinonic acid and norpinic acid respectively. The mass concentrations of *cis*-pinonic acid, norpinonic acid and norpinic acid were calculated from the sum concentrations of the related ions.

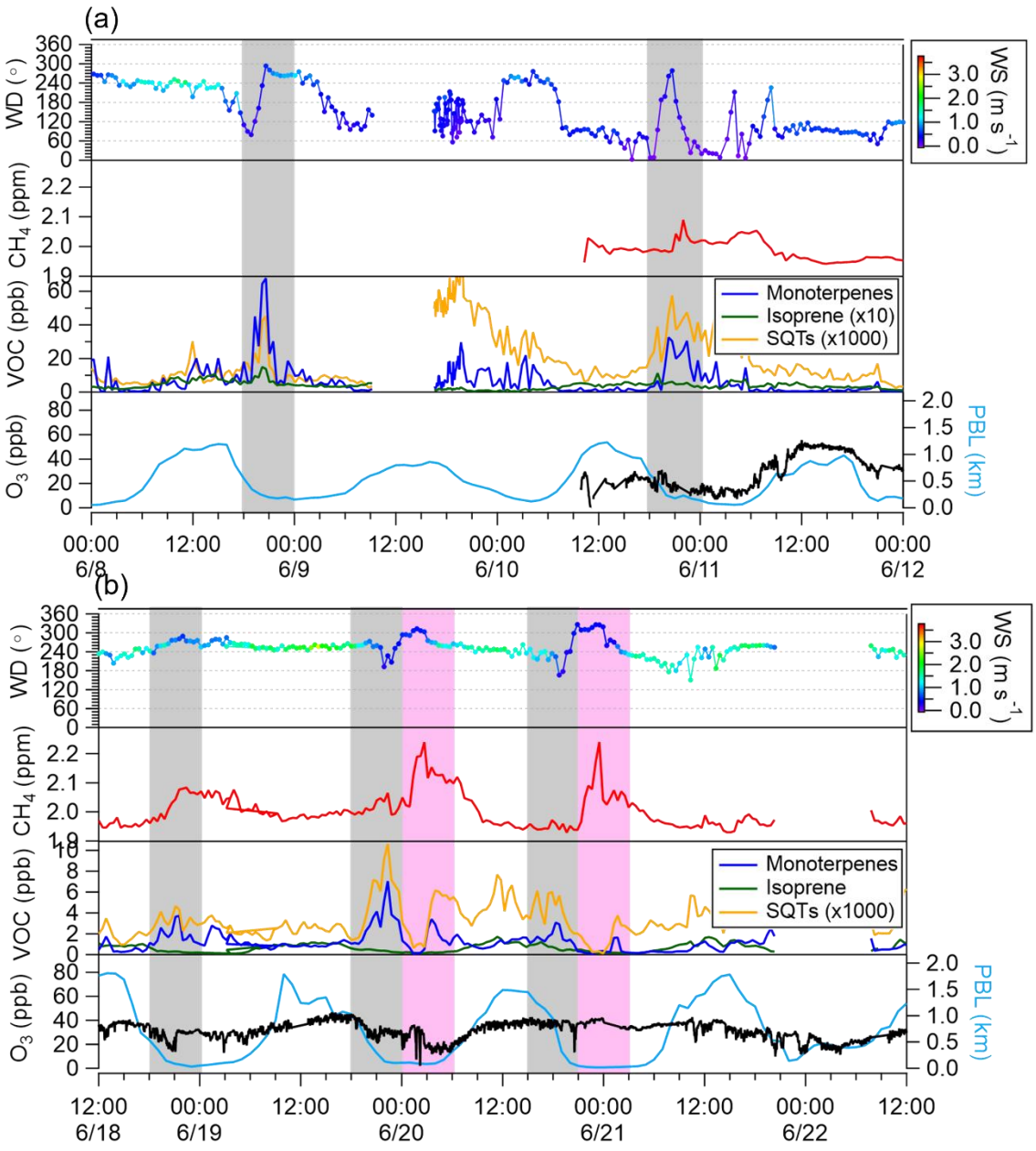

Figure S9. Time series of WD colored by the WS, CH_4, isoprene, monoterpenes and sesquiterpenes, O_3 concentrations and PBL heights during (a) 0:00 8th June-0:00 12th of June and (b) 12:00 18th of June-12:00 22nd of June. The grey and pink shaded areas are marked for the cases with rapid increases of CH_4 and monoterpene concentrations respectively.

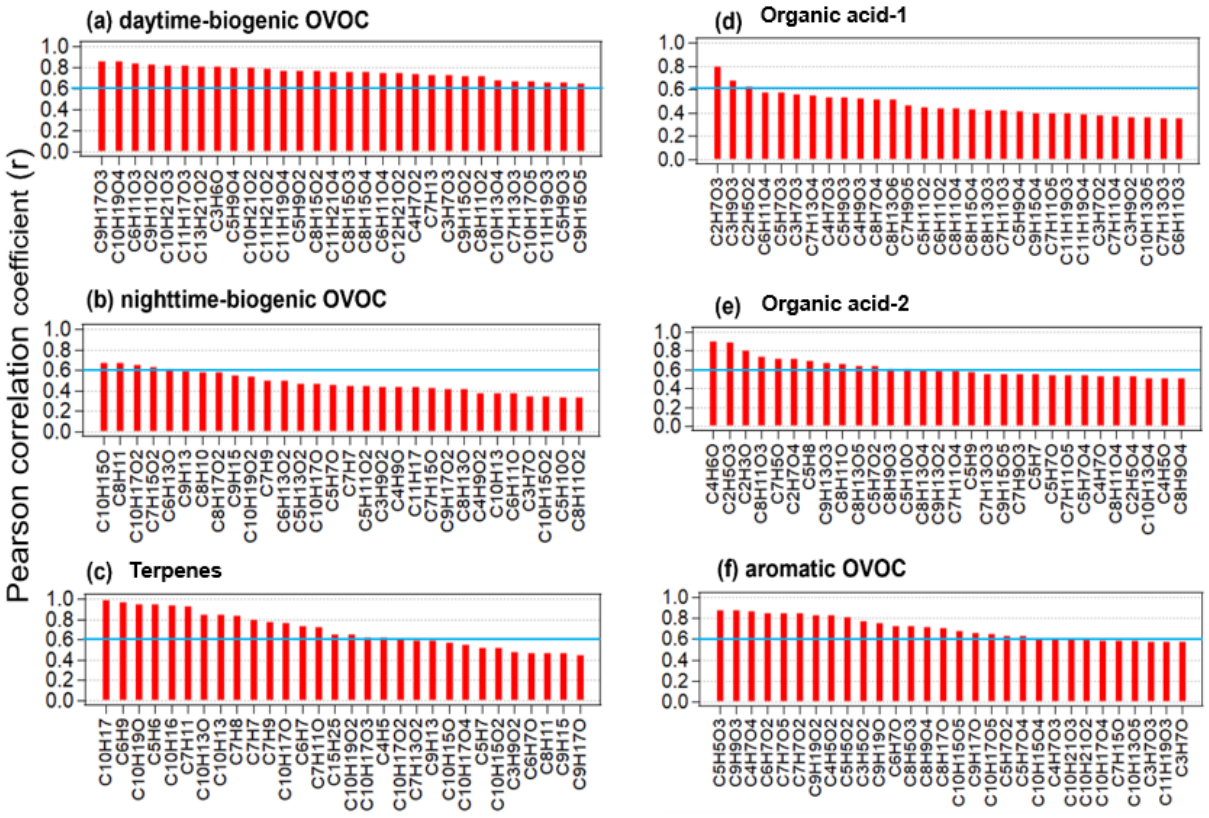

159

160 **Figure S10**. Results of the correlation analysis of six VOC factors resolved from the PMF analysis
161 of Vocus-PTR-ToF-MS mass spectral data with all VOC ions sorting by correlation coefficient.
162 The blue lines mark at r = 0.6 to indicate relatively good correlations.

163

164

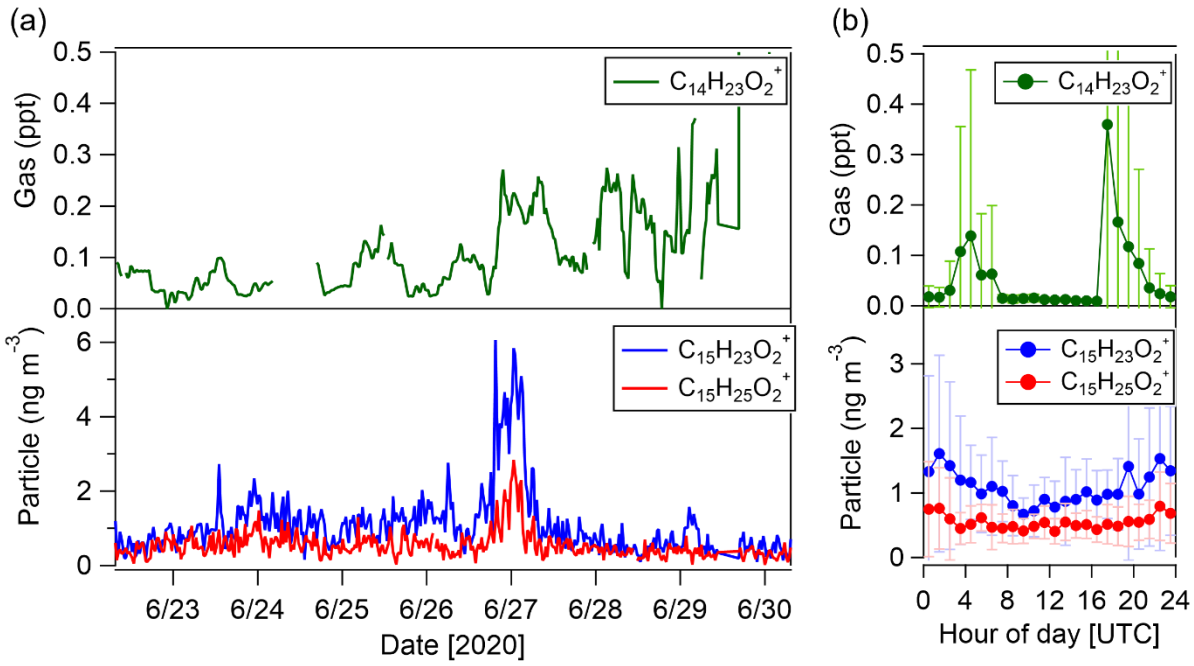

165

166 **Figure S11.** Time series of sesquiterpene oxidation products (a) $C_{14}H_{23}O_2$+ in gas phase measured
167 by the Vocus-PTR-ToF-MS and $C_{15}H_{23}O_2^+$ and $C_{15}H_{25}O_2^+$ in particle phase measured by the
168 CHARON-PTR-ToF-MS, and (b) their diurnal variations.

169

170

171

172

173

174

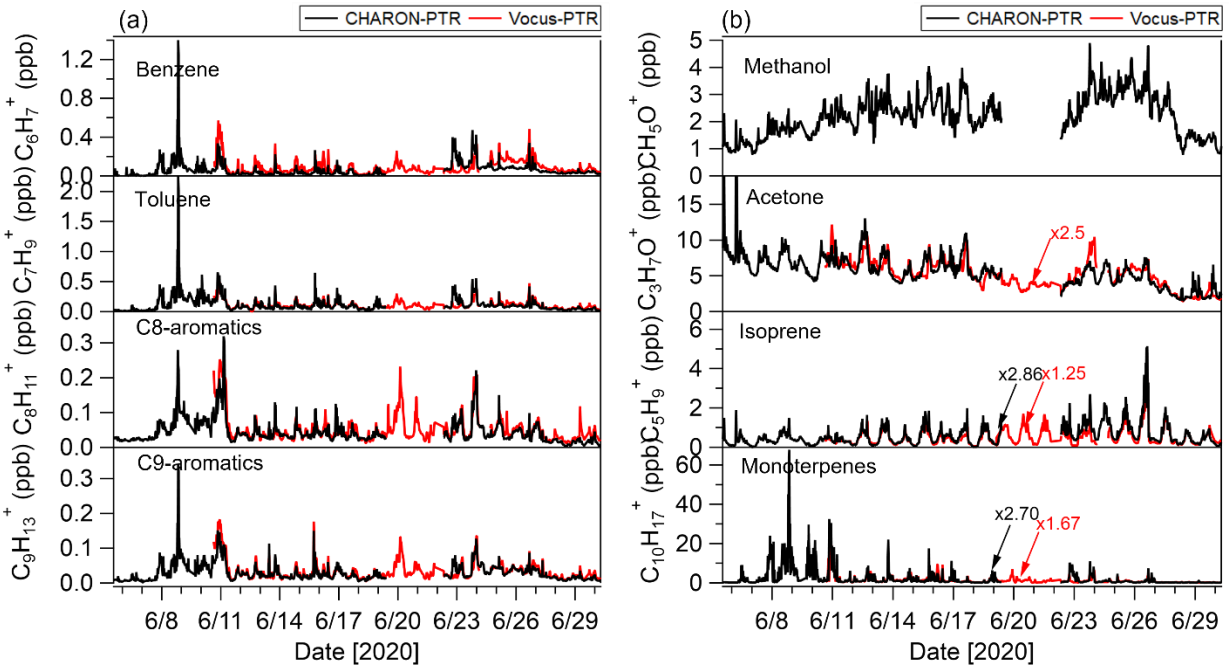

Figure S12. Comparisons of VOCs measured by CHARON-PTR-ToF-MS and Vocus-PTR-ToF-MS: (a) aromatic hydrocarbons, (b) methanol, acetone, isoprene and monoterpenes. The data of $C_5H_9^+$ and $C_{10}H_{17}^+$ were scaled to obtain the concentrations of isoprene and monoterpenes based on their fragmentation patterns in CHARON-PTR-ToF-MS and Vocus-PTR-ToF-MS.

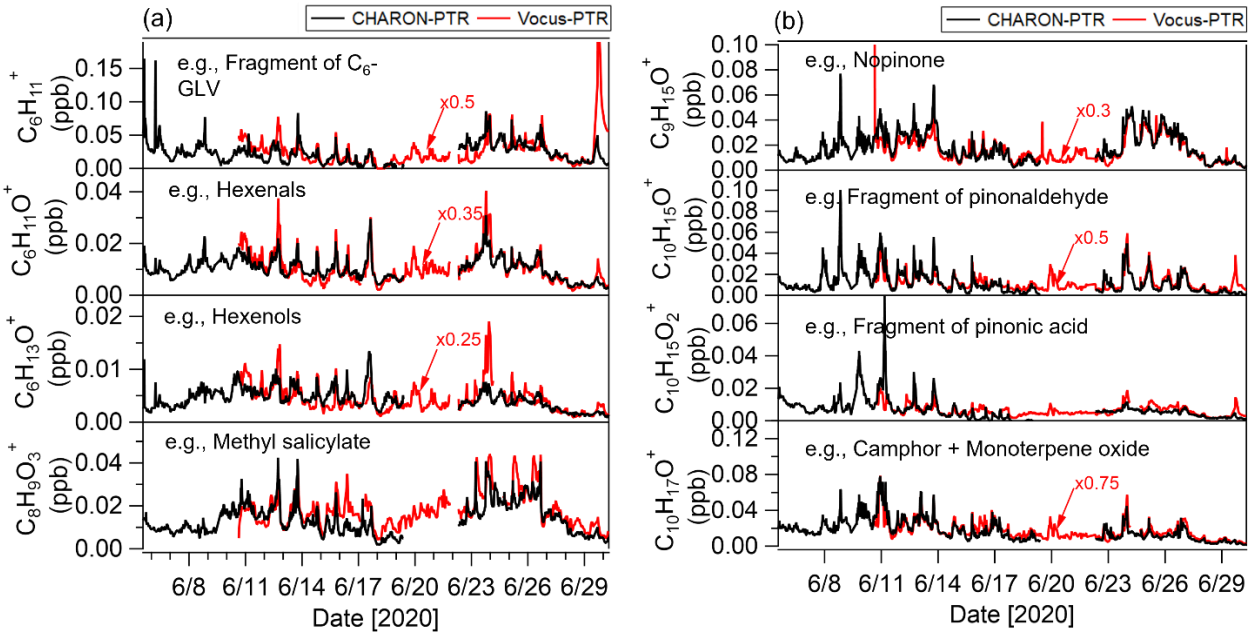

Figure S13. Comparisons of VOCs measured by CHARON-PTR-ToF-MS and Vocus-PTR-ToF-MS: (a) VOC ions related to green leaf volatiles (GLV), (b) VOC ions related to monoterpene oxidation products. The Vocus-PTR-ToF-MS data was scaled for comparison.

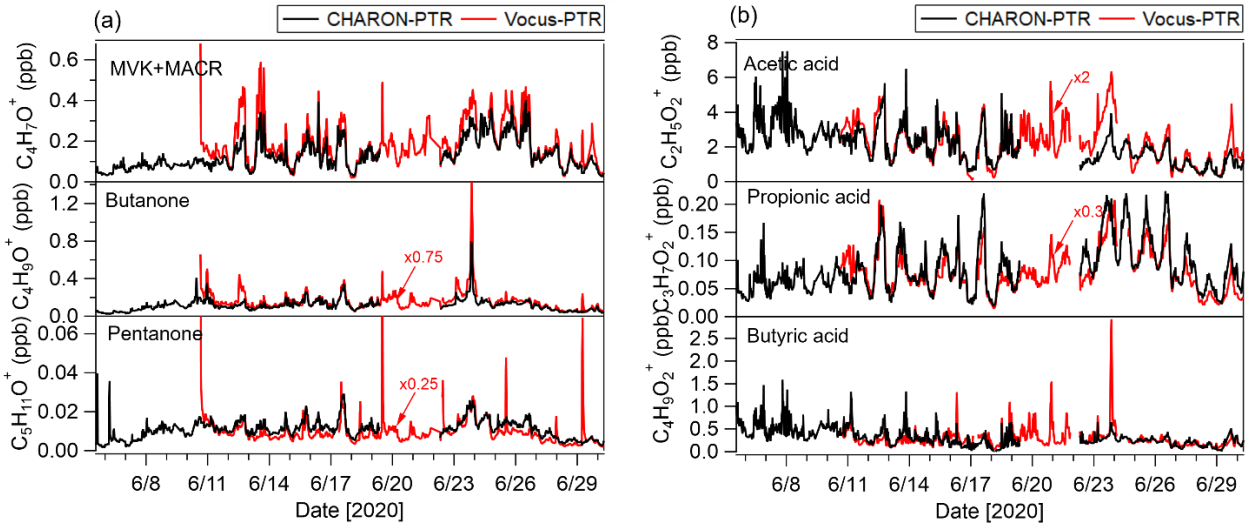

Figure S14. Comparisons of VOCs measured by CHARON-PTR-ToF-MS and Vocus-PTR-ToF-MS: (a) ketones including methyl vinyl ketone + methacrolein (MVK+MACR), butanone, pentanone and (b) acids including acetic acid, propionic acid, butyric acid. The Vocus-PTR-ToF-MS data was scaled for comparison.

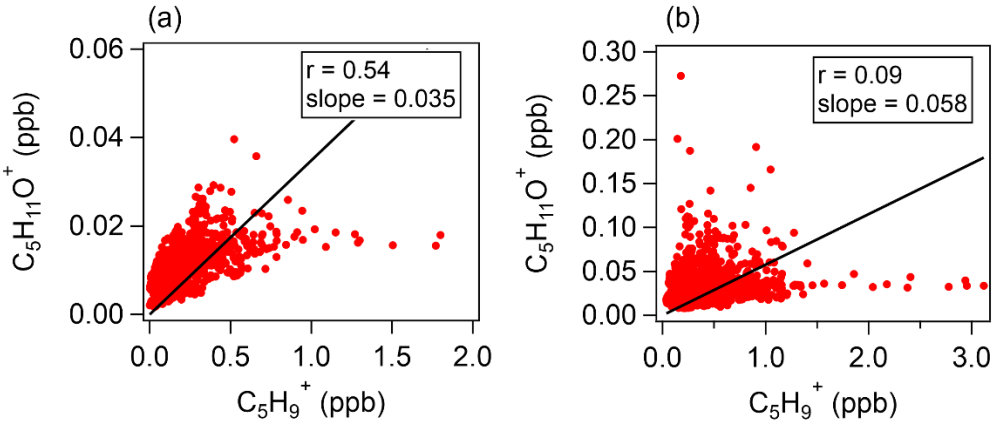

191

192 **Figure S15.** Correlation between gaseous $C_5H_{11}O^+$ and $C_5H_9^+$ measured by (a) CHARON-PTR-

193 ToF-MS and (b) Vocus-PTR-ToF-MS.

194

195

References

Bosque, R. and Sales, J.: Polarizabilities of Solvents from the Chemical Composition, Journal of Chemical Information and Computer Sciences, 42, 1154-1163, 10.1021/ci025528x, 2002.

Coggon, M. M., Stockwell, C. E., Claflin, M. S., Pfannerstill, E. Y., Lu, X., Gilman, J. B., Marcantonio, J., Cao, C., Bates, K., Gkatzelis, G. I., Lamplugh, A., Katz, E. F., Arata, C., Apel, E. C., Hornbrook, R. S., Piel, F., Majluf, F., Blake, D. R., Wisthaler, A., Canagaratna, M., Lerner, B. M., Goldstein, A. H., Mak, J. E., and Warneke, C.: Identifying and correcting interferences to PTR-ToF-MS measurements of isoprene and other urban volatile organic compounds, EGUsphere, 2023, 1-41, 10.5194/egusphere-2023-1497, 2023.

Gioumousis, G. and Stevenson, D. P.: Reactions of Gaseous Molecule Ions with Gaseous Molecules. V. Theory, The Journal of Chemical Physics, 29, 294-299, 10.1063/1.1744477, 1958.

Karl, T., Hansel, A., Cappellin, L., Kaser, L., Herdlinger-Blatt, I., and Jud, W.: Selective measurements of isoprene and 2-methyl-3-buten-2-ol based on NO⁺ ionization mass spectrometry, Atmos. Chem. Phys., 12, 11877-11884, 10.5194/acp-12-11877-2012, 2012.

Leglise, J., Müller, M., Piel, F., Otto, T., and Wisthaler, A.: Bulk Organic Aerosol Analysis by Proton-Transfer-Reaction Mass Spectrometry: An Improved Methodology for the Determination of Total Organic Mass, O:C and H:C Elemental Ratios, and the Average Molecular Formula, Analytical Chemistry, 91, 12619-12624, 10.1021/acs.analchem.9b02949, 2019.

Müller, M., Eichler, P., D'Anna, B., Tan, W., and Wisthaler, A.: Direct Sampling and Analysis of Atmospheric Particulate Organic Matter by Proton-Transfer-Reaction Mass Spectrometry, Analytical Chemistry, 89, 10889-10897, 10.1021/acs.analchem.7b02582, 2017.

Pfannerstill, E. Y., Arata, C., Zhu, Q., Schulze, B. C., Woods, R., Seinfeld, J. H., Bucholtz, A., Cohen, R. C., and Goldstein, A. H.: Volatile organic compound fluxes in the agricultural San Joaquin Valley – spatial distribution, source attribution, and inventory comparison, Atmos. Chem. Phys., 23, 12753-12780, 10.5194/acp-23-12753-2023, 2023.

Piel, F., Müller, M., Winkler, K., Skytte af Sätra, J., and Wisthaler, A.: Introducing the extended volatility range proton-transfer-reaction mass spectrometer (EVR PTR-MS), Atmos. Meas. Tech., 14, 1355-1363, 10.5194/amt-14-1355-2021, 2021.

Su, T. and Chesnavich, W. J.: Parametrization of the ion–polar molecule collision rate constant by trajectory calculations, The Journal of Chemical Physics, 76, 5183-5185, 10.1063/1.442828, 1982.

Yuan, B., Koss, A. R., Warneke, C., Coggon, M., Sekimoto, K., and de Gouw, J. A.: Proton-Transfer-Reaction Mass Spectrometry: Applications in Atmospheric Sciences, Chemical Reviews, 117, 13187-13229, 10.1021/acs.chemrev.7b00325, 2017.